Selective N$_2$ Adsorption via Backbonding in a Vanadium(II) Metal–Organic Framework

David E. Jaramillo[1#], Douglas A. Reed[1#], Henry Z. H. Jiang[1], Julia Oktawiec[1], Michael W. Mara[1], Alexander C. Forse[1,2,3], Daniel J. Lussier[1,4], Ryan A. Murphy[1], Marc Cunningham[3], Valentina Colombo[5], David K. Shuh[4], Jeffrey A. Reimer[3,6], Jeffrey R. Long[1,3,6]*

[1] Department of Chemistry, University of California, Berkeley, California 94720, USA.
[2] Berkeley Energy and Climate Institute, University of California, Berkeley, California 94720, USA.
[3] Department of Chemical and Biomolecular Engineering, University of California, Berkeley, California 94720, USA.
[4] Chemical Sciences Division, Lawrence Berkeley National Laboratory, Berkeley, CA 94720 USA.
[5] Dipartimento di Chimica, Università di Milano, 20133 Milan, Italy.
[6] Materials Sciences Division, Lawrence Berkeley National Laboratory, Berkeley, California 94720, USA.
[#]These authors contributed equally to this work

Industrial processes prominently feature π-acidic gases, and an adsorbent capable of selectively interacting with these molecules could enable a number of important chemical separations[1–4]. In nature, enzymes, and correspondingly their synthetic analogues, use accessible, reducing metal centers to bind and even activate weakly π-acidic species such as N$_2$ through backbonding interactions[5–7], and incorporation of similar moieties into a porous material should give rise to a new mechanism of adsorption for these gaseous substrates[8]. However, synthetic challenges have prevented realization of such a material. Here, we report a metal–organic framework featuring exposed vanadium(II) centers with an electronic configuration and 3d-orbital energies conducive to the back-donation of electron density to weak π-acids, thereby enabling highly selective adsorption. This new adsorption mechanism, together with the presence of a high concentration of available adsorption sites, results in record N$_2$ capacities and selectivities for the removal of N$_2$ from mixtures with CH$_4$, while further enabling the separation of olefins from paraffins at elevated temperatures. Ultimately, incorporating such π-basic metal centers into tunable porous materials offers a new handle for capturing and activating key molecular species within next-generation adsorbents.

The implementation of adsorbent-based technology stands as a promising route toward mitigating the high energy and emission costs associated with current industrial chemical

separations[1,2]. While most separation processes exploit volatility differences to impart selectivity, requiring energetically costly operating conditions, porous materials are capable of separating gases based on various chemical handles and thus can operate at more moderate pressures and temperatures[2]. However, current adsorbents typically only distinguish adsorbates based on differences in polarizability, size, or shape, and remain largely ineffective for mixtures that lack these particular distinctions. Many industrially relevant gases, such as H_2, N_2, O_2, alkenes, alkynes, and CO, feature low-energy orbitals of π-symmetry capable of accepting electron density, but an adsorbent that effectively leverages this property for energy-efficient separations has yet to be realized. The design of a material with exposed metal sites capable of backbonding to an adsorbate would introduce π-basicity as a handle for imparting selectivity, potentially enabling a host of new separations of industrially relevant mixtures.

Metal–organic frameworks, a class of crystalline and highly porous materials, have emerged as strong candidates for replacing traditional solid adsorbents[9–13]. These structures are built of metal nodes connected through multitopic organic linkers, and their surface functionalities can be chemically tuned to control adsorption properties. A prominent feature among metal–organic frameworks offering superior adsorption characteristics is the presence of coordinatively-unsaturated metal centers. Due to the typical metal ions and weak ligand field linkers used, this approach typically results in exposed Lewis-acidic metal sites that are capable of accepting electron density from various adsorbates, enabling polarizability-based separations[14,15]. However, such materials are unable to distinguish gases on the basis of backbonding. The separation of mixtures where π-acidity serves as a more suitable handle requires a material with exposed, reducing metal centers with the proper electron configuration that can donate electron density into an adsorbate π* orbital, as is seen in nitrogenases and its biomimetic analogues[5–7]. A hypothetical metal–organic framework containing square pyramidal vanadium(II) centers was previously proposed as an excellent candidate for backbonding-based separations[8]. Here, the electropositive and diffuse character of the vanadium 3d-orbitals promotes an effective energetic and spatial overlap with the adsorbate π* lowest unoccupied molecular orbital, leading to a selective interaction relative to non π-acids. Additionally, the d^3 configuration in this ligand geometry is optimal for strong yet reversible backbonding interactions. However, many properties of vanadium(II), such as its kinetic inertness, a large thermodynamic driving force toward oxidation, and reactivity with carboxylate-containing ligands, have thus far prohibited the isolation of a

crystalline framework material containing coordinatively-unsaturated vanadium(II) sites[16]. Although some metal–organic frameworks are known to contain metal centers with the appropriate electronic configuration for π-backbonding, the lack of diffuse orbitals or the requisite molecular orbital energies has prevented realization of an effective adsorbent for π-acidic gases[17,18].

The importance of addressing these synthetic challenges is emphasized by considering one of the most industrially expensive separations: the removal of N_2 from natural gas[19,20]. Given their similar physical properties, the separation of N_2 and CH_4 is very challenging and is currently carried out using capital- and energy-intensive cryogenic distillation. As the global energy market share of natural gas continues to increase, and as N_2-contaminated alternative sources of methane become more accessible, the development of an energy-efficient separation process is becoming increasingly important[21]. While some N_2-selective adsorbents exist, these either suffer from low equilibrium selectivity or low N_2 capacity and are therefore ineffective for large-scale practical applications[18,22]. An adsorbent with a high density of square pyramidal vanadium(II) sites could overcome these limitations by exploiting the π-acidity difference between N_2 and CH_4. Herein, we report the synthesis of the first metal–organic framework with exposed vanadium(II) sites, $V_2Cl_{2.8}$(btdd) (H$_2$btdd = bis(1*H*-1,2,3-triazolo[4,5-*b*],[4′,5′-*i*])dibenzo[1,4]dioxin), which is capable of engaging π-acidic gases via backbonding interactions. Significantly, this material exhibits a record N_2 capacity under practical working conditions, a record equilibrium selectivity for N_2 over CH_4, and facile regeneration, qualifying it as a potential candidate for incorporation in an alternative natural gas purification process. Furthermore, this backbonding capability can potentially be leveraged to separate olefins from paraffins, another energy demanding industrial separation[1,4]. Importantly, this discovery expands the molecular properties that can be targeted by solid adsorbents to discriminate gases in industrial processes.

The M_2Cl_2(btdd) structure type was identified as a promising target to synthesize the first vanadium(II)-based metal–organic framework[23,24]. The nitrogen-donor containing btdd^{2-} ligand is less likely to promote deleterious vanadium oxidation reactions observed with more common carboxylate-containing ligands. Additionally, minimal rearrangement of the metal coordination sphere should be required by starting from a vanadium chloride precursor, partially circumventing the kinetic inertness of vanadium(II). Indeed, combining VCl_2(tmeda)$_2$ (tmeda = *N,N,N′,N′*-tetramethylethylenediamine) and H$_2$btdd in *N,N*-dimethylformamide under acidic conditions affords a dark purple microcrystalline powder. The activated material is highly porous, with a

3

Brunauer-Emmett-Teller surface area of 1930 m^2/g, and Rietveld refinement of powder X-ray diffraction data yielded a structural model consistent with the formula $V_2Cl_{2.8}$(btdd) (Fig. 1). The framework features one-dimensional, 23 Å-wide hexagonal channels, with vertices decorated by vanadium sites. Due to the highly reducing nature of vanadium(II), some of the metal sites are oxidized during synthesis, resulting in a framework containing approximately 60% coordinatively-unsaturated vanadium(II) sites and 40% chloride-terminated vanadium(III) sites (Supplementary Fig. 3). This metal site distribution was validated by vanadium K-edge X-ray absorption spectroscopy, which revealed an edge energy consistent with the presence of a mixture of vanadium(II) and vanadium(III) (Fig. 1d), and X-ray photoelectron spectroscopy, which indicated the presence of both bridging and terminal chloride ligands (Supplementary Fig. 4). All vanadium centers are coordinated by bridging triazolates and chlorides, with V–N bond lengths ranging from 2.11(5) to 2.29(13) Å, and equatorial V–Cl bond distances of 2.362(12) Å, consistent with mixed vanadium(II)/vanadium(III) character[25,26].

To confirm the accessibility and electron-donating ability of the square-pyramidal vanadium(II) centers, *in situ* infrared spectroscopy was used to monitor a sample dosed with CO. Upon dosing with CO at low pressure, a single band appears at 2084 cm^{-1}, indicating the presence of only one type of vanadium binding site (Fig. 1e). The band is redshifted by 59 cm^{-1} from that of free CO, in contrast to the blueshift observed in frameworks featuring Lewis-acidic open metal sites[14,18]. This result clearly demonstrates that a backbonding interaction is operative, and suggests that the material should strongly adsorb other π-acidic substrates, such as N_2.

Indeed, N_2 adsorption data reveal that $V_2Cl_{2.8}$(btdd) adsorbs significant amounts of the gas at ambient temperature. Equilibrium N_2 uptake at 25 °C exhibits an unprecedented steep rise to 1.5 mmol/g at just 50 mbar, before gradually increasing to 1.9 mmol/g (>5 wt %) at 1 bar (Fig. 2a). Analysis of isotherms collected at multiple temperatures afforded an isosteric heat of adsorption of −56 kJ/mol, the largest value yet reported for a porous material exhibiting reversible N_2 binding. This is consistent with the computationally predicated value of –49 kJ/mol for the hypothetical material V_2(dobdc) ($dobdc^{4-}$ = 2,5-dioxido-1,4-benzenedicarboxylate) (ref. 8).

The mechanism of N_2 adsorption in $V_2Cl_{2.8}$(btdd) was probed through a variety of techniques. Analysis of powder X-ray diffraction data collected on a sample dosed with 700 mbar of N_2 revealed a linear, end-on binding mode for N_2 with a V–N separation of 2.12(7) Å (Fig. 2d). Notably, this bond distance is the shortest metal–N_2 interaction reported amongst metal–organic

frameworks[8,27], and represents the first structurally characterized example of N_2 binding to a single vanadium(II) center. Nitrogen adsorption in $V_2Cl_{2.8}$(btdd) was also monitored using *in situ* infrared spectroscopy (Fig. 2b). Upon dosing 80 mbar of N_2, a single, isotopically-sensitive N–N stretching band appears at 2290 cm^{-1}. This value is redshifted by 41 cm^{-1} with respect to gas-phase N_2, consistent with a computationally predicted weak field vanadium(II)–N_2 interaction, free of solvent and cation effects[8]. Finally, solid-state magic-angle spinning (MAS) ^{15}N-NMR spectroscopy data was collected for a $V_2Cl_{2.8}$(btdd) sample dosed with $^{15}N_2$ (Fig. 2c). The signal observed at 267 ppm is significantly broadened and paramagnetically shifted from free, gas-phase N_2 (307 ppm), in contrast to what has been observed previously for Lewis-acidic adsorbents[28] and consistent with the transfer of unpaired electron spin density from vanadium to N_2. Taken together, these data confirm that the binding of N_2 to the vanadium centers involves a π-backbonding interaction.

The substantial N_2 uptake resulting from this binding mechanism, particularly at low pressures, should enable exceptional performance in the adsorption of N_2 for industrial applications. Removing N_2 from mixtures with CH_4, one of the largest commercial separations involving N_2, is necessary for processing contaminated natural gas reserves. In particular, pipeline quality standards require a total inert gas content of less than 4%, with N_2 levels typically below 2% (refs. 3, 19, 20). Consequently, a viable adsorbent must maximize both capacity and selectivity for N_2 over CH_4 at low N_2 partial pressures. A comparison of $V_2Cl_{2.8}$(btdd) to previously reported materials for N_2 capture[18,22] reveals that the new adsorption mechanism allows for the highest uptake for all pressures measured at near-ambient temperatures. Additionally, the performance of $V_2Cl_{2.8}$(btdd) at low pressures far surpasses that of all reported materials. Indeed, the previous benchmark material, a chromium(III) metal–organic framework, only adsorbs ~0.25 mmol/g at 20 mbar at 10 °C (ref. 18), compared to 1.09 mmol/g at 20 mbar observed for $V_2Cl_{2.8}$(btdd) at the higher temperature of 25 °C. Even more impressive, the room-temperature N_2 uptake at 40 mbar in $V_2Cl_{2.8}$(btdd) is higher than that of any other adsorbent even at pressures up to 1 bar, highlighting its potential for this separation.

In assessing the selectivity for N_2 adsorption, a comparison to the CH_4 adsorption isotherm collected at 25 °C shows that $V_2Cl_{2.8}$(btdd) adsorbs substantially more N_2 at all pressures measured (Fig. 3a). While CH_4 adsorbs within $V_2Cl_{2.8}$(btdd) with a considerable binding enthalpy of −35 kJ/mol, similar to that predicted for V_2(dobdc) (ref. 8), its adsorption profile relative to that of N_2

suggests that the framework should exhibit considerable selectivity for N_2. Indeed, N_2/CH_4 selectivity values calculated using ideal adsorbed solution theory (IAST) are exceptional for low N_2 concentrations at 1 bar total pressure (Fig. 3b). For example, for a 20:80 N_2:CH_4 mixture at 25 °C, the selectivity is 38. This value is substantially higher than the selectivity of ~8 reported for the previous benchmark material at 10 °C, which also displays significant decreases in selectivity upon warming[18]. Notably, due to the steep rise in the N_2 adsorption isotherm, the IAST selectivity also rises considerably at lower concentrations of N_2, reaching values of 63 and 72 at 4% and 2% N_2 in CH_4, respectively. Furthermore, the material also shows a high affinity for CO_2, another key contaminant in many sources of natural gas[3], and displays selectivity with an IAST value of 37 for the industrially relevant 10:90 CO_2:CH_4 mixture (Supplementary Fig. 8). These values suggest that $V_2Cl_{2.8}$(btdd) should be capable of producing natural gas free of both N_2 and CO_2 in a single-pass separation process.

Importantly, N_2 adsorption isotherms collected at higher temperatures also exhibit a steep initial N_2 uptake, indicating that $V_2Cl_{2.8}$(btdd) should remain selective for N_2/CH_4 separations even at significantly elevated temperatures. For temperatures as high as 45 °C, the IAST selectivity values are similar to those calculated at 25 °C and they remain practically invariant at N_2 concentrations higher than 20% over this temperature range (Fig. 3b), highlighting the significance of the strong orbital-mediated V–N_2 interaction. This result is also analogous to that observed for other materials that engage in strong, chemisorptive interactions with target substrates, and in some cases such materials even display increased selectivities at higher temperatures[29]. In contrast, polarizability-driven mechanisms exhibit dramatic negative temperature effects, such as that observed for the previous benchmark chromium(III) material, for which raising the temperature from 10 to 20 °C lowers the IAST selectivity under standard conditions by over 20% (ref. 18).

We sought to investigate the applicability of this new backbonding adsorption mechanism to the separation of olefins from paraffins, such as the separation of ethylene from ethane and propylene from propane, which are carried out on enormous scales using cryogenic distillation[1,4]. Metal–organic frameworks containing coordinatively-unsaturated metal centers have previously been studied for these separations[11,30]. However, while these materials are able to perform effectively at room temperature, their selectivity diminishes substantially at higher temperatures that can align with olefin-paraffin production processes[4,31]. We first monitored the mechanism of olefin adsorption in $V_2Cl_{2.8}$(btdd) by *in situ* dosing of propylene while collecting infrared spectra.

The room-temperature spectrum features a redshifted C=C stretch at 1620 cm^{-1}, the first such example for propylene adsorption in a metal–organic framework (Supplementary Fig. 9). This suggests that the vanadium centers engage in a backbonding interaction with the olefin π* orbitals. Analysis of single-component ethylene and propylene adsorption isotherms collected at multiple temperatures further reveals that the gases adsorb with similar binding enthalpies of −68 and −67 kJ/mol, respectively. These results again support adsorption via a backbonding mechanism, in contrast to traditional Lewis-acidic binding sites that operate via a polarizability-based mechanism and bind propylene substantially more strongly than ethylene[11].

Importantly, as a consequence of π-backbonding, $V_2Cl_{2.8}$(btdd) retains strong binding affinities for olefins at high temperatures. Indeed, the ethylene adsorption isotherm collected at 80 °C shows a steep and substantial uptake, and notably the adsorption remains fully reversible even at lower temperatures (Fig. 4a, Supplementary Fig. 12). In contrast, ethane adsorption isotherms are more shallow at all temperatures measured. For a 50:50 ethylene:ethane mixture, the IAST selectivity notably increases with temperature, reaching a value of 6.9 at 80 °C (Fig. 4b). To our knowledge, this represents the first reported instance of selectivity increasing with temperature for this industrially relevant mixture, and, importantly, the material retains a high ethylene capacity even at 80 °C. The temperature dependence of this selectivity could allow for operation under much more energetically favorable conditions[4,31], and thus this backbonding mechanism may be applicable for realistic industrial separations. In addition, the record ethylene selectivity values exhibited by the framework at elevated temperatures and low ethylene concentrations (*e.g.*, 17 for a 5:95 ethylene:ethane mixture at 80 °C) suggest that this material may be particularly effective for the separation of ethylene in ethane-rich feeds.

Realization of a material with a high-density of reducing, coordinatively-unsaturated vanadium(II) centers capable of strong yet reversible backbonding interactions, has unleashed an extraordinary potential for binding of π-acidic gases. Indeed, $V_2Cl_{2.8}$(btdd) exemplifies valuable design principles for next generation adsorbents capable of exploiting differences in adsorbate molecular orbitals to impart selectivity and potentially even new reactivity that is yet to be explored.
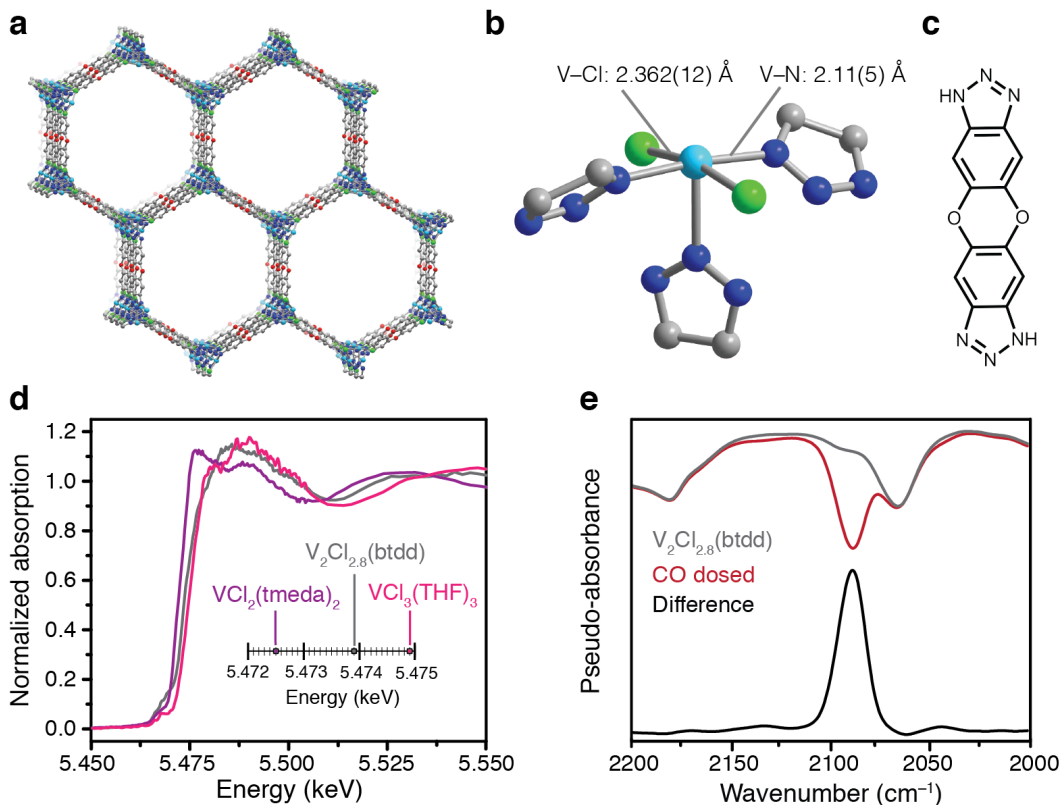
Figure 1 | Structural and spectroscopic characterization of V₂Cl₂.₈(btdd)

a, b, Portion of the $V_2Cl_{2.8}$(btdd) structure **(a)**, as determined from analysis of powder X-ray diffraction data, and the first coordination sphere of a five-coordinate vanadium center within the framework **(b)**. Cyan, green, blue, red, and grey spheres represent V, Cl, N, O, and C, atoms respectively. Terminal chloride ligands and H atoms have been omitted for clarity. **c,** Structure of the organic linker H_2btdd. **d,** Vanadium *K*-edge X-ray absorption spectra collected for $V_2Cl_{2.8}$(btdd) (grey), a vanadium(II) reference V_2Cl_2(tmeda)$_2$ (purple), and a vanadium(III) reference VCl_3(THF)$_3$ (pink, THF = tetrahydrofuran). The inset depicts edge energies determined at the half-maximum of the rising edge. **e,** Infrared spectra collected at 25 °C for activated $V_2Cl_{2.8}$(btdd) (grey) and $V_2Cl_{2.8}$(btdd) dosed with 33 mbar of CO (red), with the difference between these two spectra shown in black.

8
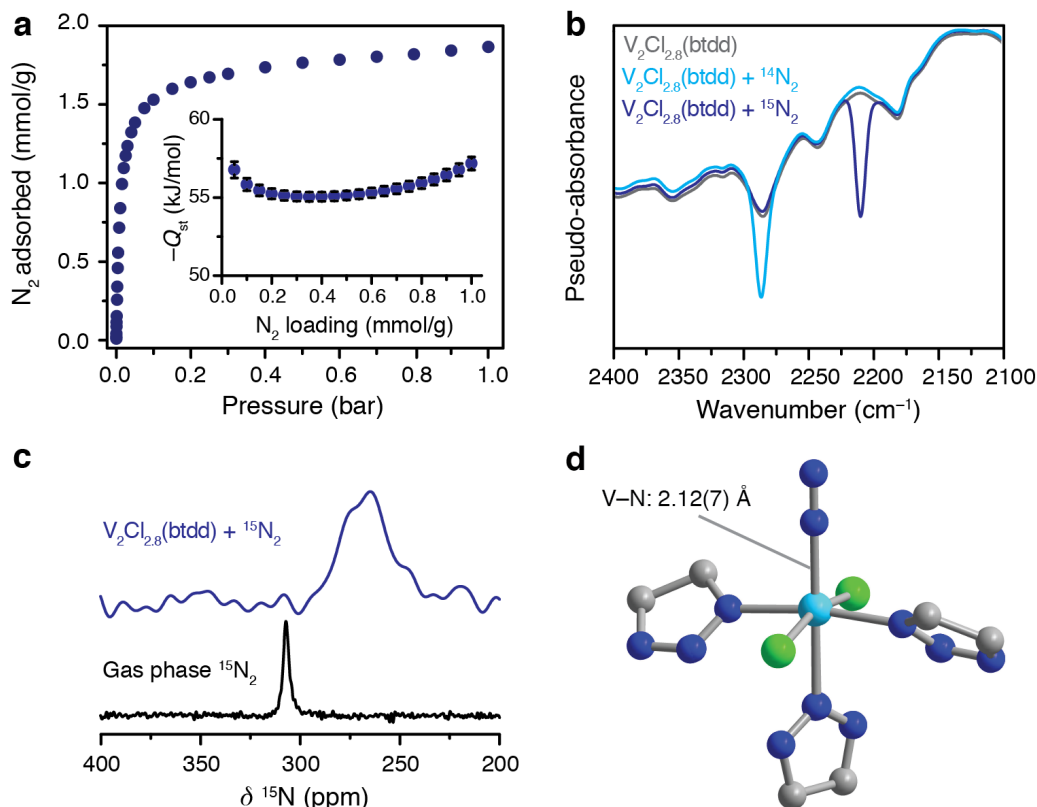
Figure 2 | Characterization of the V−N₂ interaction in V₂Cl₂.₈(btdd)

a, Nitrogen adsorption isotherm collected at 25 °C, with inset showing the isosteric heat of N_2 adsorption (error bars are shown in black). **b,** Infrared spectra for $V_2Cl_{2.8}$(btdd) collected at 25 °C under vacuum (grey), upon dosing with 80 mbar of $^{14}N_2$ (cyan), and upon dosing with 85 mbar of $^{15}N_2$ (blue). **c,** Nitrogen-15 nuclear magnetic resonance (NMR) spectra collected for free, gas-phase $^{15}N_2$ at 700 mbar (black) and for $V_2Cl_{2.8}$(btdd) dosed with 770 mbar of $^{15}N_2$ (blue) at room temperature. The spectrum of the solid sample was collected using magic angle spinning at 15 kHz. **d,** Structure of a single vanadium site in $V_2Cl_{2.8}$(btdd) upon dosing with 700 mbar of N_2, as determined from analysis of powder X-ray diffraction data. Cyan, green, blue, and grey spheres represent V, Cl, N, and C atoms, respectively; a 40%-occupied terminal chloride ligand has been omitted.
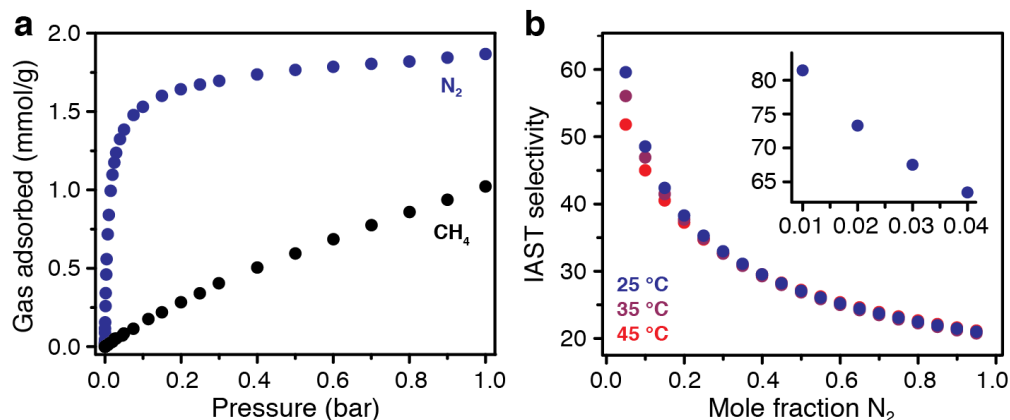
Figure 3 | Assessment of N$_2$/CH$_4$ selectivity

a, Adsorption isotherms for N$_2$ (blue) and CH$_4$ (black) collected at 25 °C in V$_2$Cl$_{2.8}$(btdd). **b,** IAST selectivity values calculated at 25, 35, and 45 °C for varying N$_2$:CH$_4$ ratios at a total pressure of 1 bar. The inset highlights the IAST selectivity values at low N$_2$ concentrations.
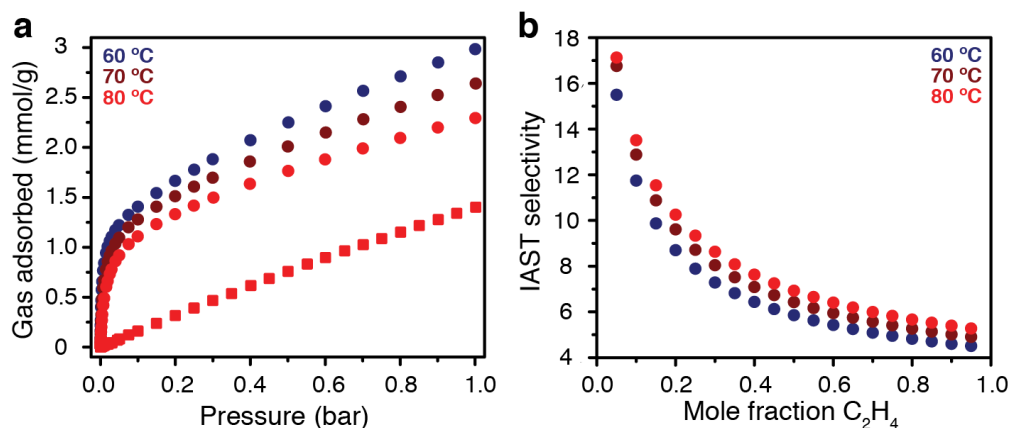

Figure 4 | Selective ethylene capture at high temperatures

a, High-temperature ethylene and ethane adsorption isotherms collected at various temperatures for V$_2$Cl$_{2.8}$(btdd). Circles and squares represent ethylene and ethane isotherms, respectively. **b,** IAST selectivity values calculated at 60, 70, and 80 °C for varying ethylene:ethane ratios at a total pressure of 1 bar.

References:

1. Sholl, D. S., Lively, R. P. Seven chemical separations to change the world. *Nature* **532**, 435–438 (2016).
2. U.S. Department of Energy. *Materials Separation Technology: Energy and Emission Reduction Opportunities* (2005).
3. Rufford, T. E., Smart, S., Watson, G. C., Graham, B. F., Boxall, J., Da Costa, J. D., May, E. F. The removal of CO_2 and N_2 from natural gas: A review of conventional and emerging process technologies. *J. Pet. Sci. Eng.* **94**, 123–154 (2012).
4. Eldridge, R. B. Olefin/Paraffin separation technology: a review. *Ind. Eng. Chem. Res.* **32**, 2208–2212 (1993).
5. Hoffman, B. M., Lukoyanov, D., Yang, Z.-Y., Dean, D. R., Seefeldt, L. C. Mechanism of nitrogen fixation by nitrogenase: the next stage. *Chem. Rev.* **114**, 4041–4062 (2014).
6. Crans, D. C., Smee, J. J., Gaidamauskas, E., Yang, L. The chemistry and biochemistry of vanadium and the biological activities exerted by vanadium compounds. *Chem. Rev.* **104**, 840–902 (2004).
7. MacKay, B. A., Fryzuk, M. D. Dinitrogen coordination chemistry: on the biomimetic borderlands. *Chem. Rev.* **104**, 385–402 (2004).
8. Lee, K., Isley III, W. C., Dzubak, A. L., Verma, P., Stoneburner, S. J., Lin, L. C., Howe, J. D., Bloch, E. D., Reed, D. A., Hudson, M. R., Brown, C. M., Long, J. R., Neaton, J. B., Smit, B., Cramer, C. J., Truhlar, D. G., Gagliardi, L. Design of a metal–organic framework with enhanced back bonding for separation of N_2 and CH_4. *J. Am. Chem. Soc.* **136**, 698–704 (2014).
9. Furukawa, H., Cordova, K. E., O'Keefe, M., Yaghi, O. M. The chemistry and applications of metal–organic frameworks. *Science* **341,** 1230444 (2013).
10. Li, J. R., Kuppler, R. J., Zhou, H. C. Selective gas adsorption and separation in metal–organic frameworks. *Chem. Soc. Rev.* **38,** 1477–1504 (2009).
11. Bloch, E. D., Queen, W. L., Krishna, R., Zadrozny, J. M., Brown, C. M., Long, J. R. Hydrocarbon separations in a metal–organic framework with open iron(II) sites. *Science* **335**, 1606–1610 (2012).
12. Cadieu, A., Adil, K., Bhatt, P. M., Belmabkhout, Y., Eddaoudi, M. A metal–organic framework-based splitter for separating propylene from propane. *Science* **353**, 137–140 (2016)
13. Herm, Z. R., Wiers, B. M., Mason, J. A., van Baten, J. M., Hudson, M. R., Zajdel, P., Brown, C. M., Masciocchi, N., Krishna, R., Long, J. R., Separation of hexane isomers in a metal–organic framework with triangular channels. *Science* **340**, 960–962 (2013).
14. Bloch, E. D., Hudson, M. R., Mason, J. A., Chavan, S., Crocellà, V., Howe, J. D., Lee, K., Dzubak, A. L., Queen, W. L., Zadrozny, J. M., Geier, S. J., Lin, L. C., Gagliardi, L., Smit, B., Neaton, J. B., Bordiga, S., Brown, C. M., Long, J. R. Reversible CO binding enables tunable CO/H_2 and CO/N_2 separations in metal–organic frameworks with exposed divalent metal cations. *J. Am. Chem. Soc.* **136**, 10752–10761 (2014).

15. Poloni, R., Lee, K., Berger, R. F., Smit, B., Neaton, J. B. Understanding trends in CO_2 adsorption in metal–organic frameworks with open-metal sites. *J. Phys. Chem. Lett.* **5**, 861–865 (2014).

16. Cotton, F. A., Extine, M. W., Falvello, L. R., Lewis, D. B., Lewis, G. E., Murillo, C. A., Schwotzer, W., Tomas, M., Troup, J. M. Four compounds containing oxo-centered trivanadium cores surrounded by six μ,η^2-carboxylato groups. *Inorg. Chem.* **25**, 3505–3512 (1986).

17. Denysenko, D., Grzywa, M., Jelic, J., Reuter, K., Volkmer, D. Scorpionate-type coordination in MFU-4*l* metal–organic frameworks: small-molecule binding and activation upon the thermally activated formation of open metal sites. *Angew. Chem., Int. Ed.* **53**, 5832–5836 (2014).

18. Yoon, J. W., Chang, H., Lee, S. J., Hwang, Y. K., Hong, D. Y., Lee, S. K., Lee, J. S., Jang, S., Yoon, T. U., Kwac, K., Jung, Y., Pillai, R. S., Faucher, F., Vimont, A., Daturi, M., Férey, G., Serre, C., Maurin, G., Bae, Y. S., Chang, J. S. Selective nitrogen capture by porous hybrid materials containing accessible transition metal ion sites. *Nat. Mater.* **16**, 526–531 (2017).

19. Caventi, S., Grande, C. A., Rodrigues, A. E. Separation of $CH_4/CO_2/N_2$ mixtures by layered pressure swing adsorption for upgrade of natural gas. *Chem. Eng. Sci.* **61**, 3893–3906 (2006).

20. Lokhandwala, K. A., Pinnau, I., He, Z., Amo, K. D., DaCosta, A. R., Wijmans, J. G., Baker, R. W. Membrane separation of nitrogen from natural gas: A case study from membrane synthesis to commercial deployment. *J. Membr. Sci.* **346**, 270–279 (2010).

21. Saha, D., Grappe, H. A., Chakraborty, A., Orkoulas, G. Postextraction, separation, on-board storage, and catalytic conversion of methane in natural gas: a review. *Chem. Rev.* **116**, 11436–11499 (2016).

22. Kuznicki, S. M., Bell, V. A., Nair, S., Hillhouse, H. W., Jacubinas, R. M., Braunbarth, C. M., Toby, B. H., Tsapatsis, M. A titanosilicate molecular sieve with adjustable pores for size-selective adsorption of molecules. *Nature* **412**, 720–724 (2004).

23. Reed, D. A., Keitz, B. K., Oktawiec, J., Mason, J. A., Runčevski, T., Xiao, D. J., Darago, L. E., Crocellà, V., Bordiga, S., Long, J. R. A spin transition mechanism for cooperative adsorption in metal–organic frameworks. *Nature* **550**, 96-100 (2017).

24. Rieth, A. J., Tulchinsky, Y., Dincă, M. High and reversible ammonia uptake in mesoporous metal–organic frameworks with open Mn, Co, and Ni sites. *J. Am. Chem. Soc.* **138**, 9401–9404 (2016)

25. Bechlars, B., D'Alessandro, D. M., Jenkins, D. M., Iavarone, A. T., Glover, S. D., Kubiak, C. P., Long, J. R. High-spin ground states via electron delocalization in mixed-valence imidazoalte-bridged divanadium complexes. *Nat. Chem.* **2**, 362–368 (2010).

26. Cotton, F. A., Duraj, S. A., Extine, M. W., Lewis, G. E., Roth, W. J., Schmulbach, C. D., Schwotzer, W. Structural studies of the vanadium(II) and vanadium(III) chloride tetrahydrofuran solvates. *J. Chem. Soc., Chem. Commun.* **23**, 1377–1378 (1983)

27. Gonzalez, M. I., Mason, J. A., Bloch, E. D., Teat, S. J., Gagnon, K. J., Morrison, G. Y., Queen, W. L., Long, J. R. Structural characterization of framework-gas interactions in the metal–organic framework Co_2(dobdc) by *in situ* single-crystal X-ray diffraction. *Chem. Sci*. **8**, 4387–4398 (2017).

28. Fonseca, A., Lledos, B., Pullumbi, P., Lignieres, J., Nagy, J. B. ^{15}N-NMR characterization and quantitative NMR determination of nitrogen adsorbed in MX zeolites. *"Porous Materials in Environmentally Friendly Processes"* in *Surface Science and Catalysis*, **125**, 229 (1999).

29. Reed, D. A., Xiao, D. J., Gonzalez, M. I., Darago, L. E., Herm, Z. R., Grandjean, F., Long, J. R. Reversible CO scavenging via adsorbate-dependent spin state transitions in an iron(II)–triazolate metal–organic framework. *J. Am. Chem. Soc.* **138**, 5594–5602 (2016).

30. Li, B., Zhang, Y., Krishna, R., Yao, K., Han, Y., Wu, Z., Ma, D., Shi, Z., Pham, T., Space, B., Liu, J., Thallapally, P. K., Liu, J., Chrzanowski, M., Ma, S. Introduction of pi-complexation into porous aromatic framework for highly selective adsorption of ethylene over ethane. *J. Am. Chem. Soc.* **136**, 8654–8660 (2014).

31. Ren, T., Patel, M., Blok, K. Olefins from conventional and heavy feedstocks: energy use in steam cracking and alternative processes. *Energy* **31**, 425–451 (2006).

Author Contributions

D.E.J., D.A.R., and J.R.L. formulated the project. D.E.J. and D.A.R. synthesized the materials. D.E.J. and D.A.R. collected and analyzed the gas adsorption data. H.Z.H.J. collected and analyzed the infrared spectra. D.E.J., J.O., and V.C. collected and analyzed the X-ray diffraction data. M.W.M., D.J.L., and D.K.S. collected and analyzed the X-ray absorption spectra. A.C.F., M.C., and J.A.R. collected and analyzed the NMR spectra. R.A.M. collected and analyzed the X-ray photoemission spectroscopy data. D.E.J., D.A.R., and J.R.L. wrote the manuscript, and all authors contributed to revising the manuscript.

separations. The University of California, Berkeley has applied for a patent on some of the technology discussed herein, on which J.R.L., D.E.J., and D.A.R. are listed as co-inventors. Correspondence and requests for materials should be addressed to J.R.L. (jrlong@berkeley.edu).

Disclaimers

The views and opinions of the authors expressed herein do not necessarily state or reflect those of the United States Government or any agency thereof. Neither the United States Government nor any agency thereof, nor any of their employees, makes any warranty, expressed or implied, or assumes any legal liability or responsibility for the accuracy, completeness, or usefulness of any information, apparatus, product, or process disclosed, or represents that its use would not infringe privately owned rights.

Methods

General synthesis and characterization methods. All synthetic procedures were performed under an argon atmosphere using standard Schlenk techniques or in an N_2-filled VAC Atmospheres glove box. Methanol was purchased from EMD Millipore Corporation as DriSolv grade, dried over 3 Å molecular sieves, and sparged with argon before use. *N,N*-dimethylformamide (DMF) was purchased from EMD Millipore Corporation as OmniSolv grade, sparged with argon, and dried with an alumina column before use. The materials $VCl_2(tmeda)_2$ (tmeda = *N,N,N′,N′*-tetramethylethylenediamine), H_2(btdd) (bis(1*H*-1,2,3-triazolo[4,5-*b*],[4′,5′-*i*])dibenzo[1,4]dioxin), and $VCl_3(THF)_3$ (THF = tetrahydrofuran) were prepared according to previously reported procedures[32–34]. Dimethylformamidium trifluoromethanesulfonate was purchased from Sigma-Aldrich and dried under vacuum prior to use. Ultrahigh-purity-grade (99.999%) He, N_2, CH_4 and CO_2, and research-purity-grade (99.99%) CO, C_2H_4, C_2H_6, and C_3H_6 were used for all gas adsorption measurements and dosing. Isotopically labelled $^{15}N_2$ (98 atom % ^{15}N) was purchased from Sigma-Aldrich and used as received. Elemental analyses for C, H and N were performed at the Microanalytical Laboratory at the University of California, Berkeley.

Synthesis of $V_2Cl_{2.8}$(btdd). A solution of $VCl_2(tmeda)_2$ (90.0 mg, 0.254 mmol) and dimethylformamidium trifluoromethanesulfonate (266 mg, 1.20 mmol) in DMF (10 mL) was added to a 20 mL borosilicate vial containing H_2(btdd) (20.0 mg, 0.0752 mmol). The mixture was heated at 120 °C, without stirring, for 10 days. The resulting dark purple powder was collected by filtration, and soaked in 10 mL of DMF at 120 °C for 24 h. The supernatant solution was decanted, another 10 mL of DMF were added, and vial was heated at 120 °C for 24 h. This process was repeated five more times so that the total time washing with DMF was 7 days. The solid was then collected by filtration, and soaked in 10 mL of methanol at 60 °C for 12 h. The supernatant solution was decanted, and the remaining powder was soaked in another 10 mL of methanol at 60 °C for 12 h. This process was repeated four more times so that the total time washing with methanol was 3 days. The resulting solid was collected by filtration, and heated at a rate of 0.2 °C/min and held at 180 °C under dynamic vacuum for 36 h, affording 20 mg of product as a dark purple powder. Elemental analysis of $[V_2Cl_{2.8}(btdd)](CH_3OH)_2$, $C_{14}H_{12}Cl_{2.8}N_6O_4V_2$: Found C, 32.76; H, 2.44; N, 15.88. Calculated: C, 31.76; H, 2.28; N, 15.87.

Gas adsorption measurements. Gas adsorption isotherms for pressures in the range 0–1 bar were measured by a volumetric method using a Micromeritics ASAP2020 or Micromeritics 3Flex gas sorption analyzer. In an N_2 filled glovebox, a typical sample of approximately 50 mg was transferred to a pre-weighed analysis tube, which was capped with a Micromeretics TranSeal and evacuated by heating at 180 °C with a ramp rate of 0.2 °C/min under dynamic vacuum until an outgas rate of less than 3 µbar/min was achieved. The evacuated analysis tube containing the degassed sample was then carefully transferred to an electronic balance and weighed again to determine the mass of sample. The tube was then transferred back to the analysis port of the gas adsorption instrument. The outgas rate was again confirmed to be less than 3 µbar/min. For all isotherms, warm and cold free space correction measurements were performed using ultrahigh-

purity He gas. Isotherms of N_2, CH_4, CO_2, C_2H_4, C_2H_6, and C_3H_6 collected at 298 to 358 K were measured in water baths equipped with a Julabo F32 circulator. N_2 isotherms collected at 77 K were measured in liquid nitrogen baths. Oil-free vacuum pumps and oil-free pressure regulators were used for all measurements to prevent contamination of the samples during the evacuation process or of the feed gases during the isotherm measurements. Langmuir surface areas were determined from N_2 adsorption data at 77 K using Micromeritics software.

Powder X-ray diffraction. Microcrystalline powder samples of $V_2Cl_{2.8}$(btdd) (~5 mg) were loaded into two 1.0 mm boron-rich glass capillaries inside a glovebox under an N_2 atmosphere. The capillaries were attached to a gas cell, which was connected to the analysis port of a Micromeritics ASAP 2020 gas adsorption instrument. Both capillaries were fully evacuated at 180 °C for 12 h, one was then flame-sealed while the other capillary was dosed with N_2 to a pressure of 700 mbar, equilibrated for 2 h, and then flame-sealed. Each capillary was placed inside a Kapton tube that was sealed on both ends with epoxy.

High-resolution synchrotron X-ray powder diffraction data were collected at beamline 17-BM at the Advanced Photon Source at Argonne National Laboratory. The temperature of measurement of the capillary samples were kept at 298 K using an Oxford Cryosystems Cryostream 800. Scattered intensity was measured by a PerkinElmer a-Si flat panel detector. The average wavelength of all measurements was 0.45236 Å.

Infrared spectroscopy. Infrared spectra were collected using a Bruker Vertex 70 spectrometer equipped with a glowbar source, KBr beamsplitter, and a liquid nitrogen cooled mercury-cadmium-telluride detector. A custom-built diffuse reflectance system with a IR-accessible gas dosing cell was used for all measurements. Sample temperature was controlled by an Oxford Instruments OptistatDry TLEX cryostat, and sample atmosphere was controlled by a Micromeritics ASAP 2020Plus gas sorption analyzer. Prior to measurement, activated $V_2Cl_{2.8}$(btdd) (10 wt%) was dispersed in dry KBr in an argon-filled glovebox and evacuated at room temperature for 30 minutes. Spectra were collected *in situ* under ultrahigh-purity-grade CO, N_2, propylene, and $^{15}N_2$ (98 atom % ^{15}N, Sigma-Aldrich) at 4 cm^{-1} resolution continually until equilibrium was observed.

Solid state nuclear magnetic resonance spectroscopy. NMR spectra were collected for free gas-phase $^{15}N_2$ (98 atom % ^{15}N, Sigma-Aldrich) and $^{15}N_2$-dosed $V_2Cl_{2.8}$(btdd). For free, gas-phase $^{15}N_2$, the gas was dosed into an empty 4 mm outer diameter glass tube at 700 mbar, and then flame sealed. Gas dosing for $V_2Cl_{2.8}$(btdd) was performed on a custom gas dosing manifold described previously[35]. The rotor was packed with ~30 mg of $V_2Cl_{2.8}$(btdd) inside an N_2-filled glovebox, evacuated at room temperature for 30 minutes, and then dosed with 773 mbar of $^{15}N_2$ at room temperature with 30 minutes allowed for equilibration. For the measurement collection, all NMR spectra were recorded at 16.4 T, with a Bruker 3.2 mm magic angle spinning probe used for $^{15}N_2$-dosed $V_2Cl_{2.8}$(btdd) and a DOTY 4 mm magic angle spinning probe used for the free gas-phase $^{15}N_2$ sample. For free $^{15}N_2$ the sample was static during measurement, while $^{15}N_2$-dosed $V_2Cl_{2.8}$(btdd) was collected under magic-angle spinning at a rate of 15 kHz. Single pulse excitation

was used for all NMR experiments. All spectra were referenced to ^{15}N in glycine with a chemical shift of 33.4 ppm (ref. 36).

Vanadium *K*-edge X-ray absorption spectroscopy. Data were collected at the Advanced Light Source bending magnet microprobe beamline 10.3.2 (2.1–17 keV) with the storage ring operating at 500 mA and 1.9 GeV. The $V_2Cl_{2.8}$(btdd), VCl_2(tmeda)$_2$, and VCl_3(THF)$_3$ samples were all individually mounted under inert atmosphere conditions in an argon glovebox onto Kapton tape, sealed in multiple hermetic bags, transferred to the ALS, and measured in fluorescence mode by continuously scanning the Si (111) monochromator (Quick XAS mode). Fluorescence emission counts were recorded with a seven-element Ge solid-state detector (Canberra) and XIA electronics. All spectra were collected from 100 eV below and up to 300 eV above the edge and calibrated using a vanadium foil, with first derivative set at 5465.1 eV. All data were processed using LabVIEW custom software available at the beamline and further processed with Athena[37].

X-ray photoelectron spectroscopy. X-ray photoelectron spectroscopy (XPS) data was taken using a Perkin Elmer PHI 5600 XPS instrument. The XPS instrument was equipped with a 180° double focusing hemispherical analyzer. To prevent oxygen contamination and concomitant redox activity with samples, preparation and mounting were performed in an argon glovebox. The sample was affixed to a silicon wafer using double sided carbon tape. After mounting the wafer on the stage the sample was sealed in an airtight jar under argon. To load into the XPS, a glovebag containing the jar was sealed onto the loading chamber and subsequently purged with a high flow of argon for one hour, after which the sample was loaded into the chamber under argon.

Samples were calibrated using the aromatic carbon peak as a standard. For proper peak fitting, a Shirley background was applied to regions of interest and subtracted after peak fitting. Energy splitting of spin-orbit decoupled peaks were constrained using values obtained from VCl_2 and VCl_3 standards. All data processing and peak fitting was performed using CasaXPS.

Data and materials availability. The supplementary materials contain complete experimental and spectral details for all new compounds reported herein. Crystallographic data are available free of charge from the Cambridge Crystallographic Data Centre.

References:

32. Edema, J. J. H., Stauthamer, W., Van Bolhuis, F., Gambarotta, S., Smeets, W. J. J., Spek, A. L. Novel vanadium (II) amine complexes: a facile entry in the chemistry of divalent vanadium. Synthesis and characterization of mononuclear L$_4$VCl$_2$ [L= amine, pyridine]: X-ray structures of *trans*-(TMEDA)$_2$VCl$_2$ [TMEDA= *N, N, N', N'*-tetramethylethylenediamine] and *trans*-Mz$_2$V(py)$_2$ [Mz= *o*-C$_6$H$_4$CH$_2$N(CH$_3$)$_2$, py= pyridine]. *Inorg. Chem.* **29**, 1302–1306 (1990).
33. Denysenko, D., Grzywa, M., Tonigold, M., Streppel, B., Krkljus, I., Hirscher, M., Mugnaioli, E., Kolb, U., Hanss, J., Volkmer, D. Elucidating gating effects for hydrogen

sorption in MFU-4-type triazolate-based metal–organic frameworks featuring different pore sizes. *Chem. Eur. J.* **17**, 1837–1848 (2011).

34. Manzer, L. E., Deaton, J., Sharp, P., Schrock, R. R. Tetrahydrofuran complexes of selected early transition metals. *Inorg. Synth.*, **21**, 135–140 (1982).

35. Milner, P. J., Siegelman, R. L., Forse, A. C., Gonzalez, M. I., Runčevski, T., Martell, J. D., Reimer, J. A., Long, J. R. A diaminopropane-appended metal–organic framework enabling efficient CO_2 capture from coal flue gas via a mixed adsorption mechanism. *J. Am. Chem. Soc.* **139**, 13541–13553 (2017).

36. Bertani, P., Raya, J., Bechinger, B. [15]N chemical shift referencing in solid state NMR. *Solid State Nucl. Magn. Reson.*, **61**, 15–18 (2014).

37. Ravel, B., Newville, B. M. ATHENA, ARTEMIS, HEPHAESTUS: data analysis for X-ray absorption spectroscopy using IFEFFIT. *Journal of Synchrotron Radiation* **12,** 537 (2005).